CrystEngComm

PAPER

Cite this: DOI: 10.1039/c4ce01672f

Active site engineering in UiO-66 type metal–organic frameworks by intentional creation of defects: a theoretical rationalization†

Matthias Vandichel,*[a] Julianna Hajek,[a] Frederik Vermoortele,[b] Michel Waroquier,[a] Dirk E. De Vos[b] and Veronique Van Speybroeck*[a]

The catalytic activity of the Zr-benzenedicarboxylate (Zr-BDC) UiO-66 can be drastically increased if some BDC linkers are missing, as this removes the full coordination of the framework metal ions. As a result, metal centers become more accessible and thus more active for Lewis acid catalysed reactions. Addition of modulators (MDL) to the synthesis mixture can create more linker deficiencies (Vermoortele *et al.*, *J. Am. Chem. Soc.*, 2013, **135**, 11465) and leads to a significant increase in the catalytic activity due to the creation of a larger number of open sites. In this paper, we rationalize the function of the modulators under real synthesis conditions by the construction of free energy diagrams. The UiO-66 type materials form a very appropriate test case as the effect of addition of modulators hydrochloric acid (HCl) and trifluoroacetate (TFA) has been intensively investigated experimentally for the synthesis process and post-synthetic thermal activation. Under synthesis conditions, direct removal of BDC linkers requires a high free energy, but replacement of such linker by one or more TFA species might occur especially at high TFA : BDC ratios in the reaction mixture. Post-synthesis activation procedures at higher temperatures lead to substantial removal of the species coordinated to the Zr bricks, creating open metal sites. A mechanistic pathway is presented for the dehydroxylation process of the hexanuclear Zr cluster. For the citronellal cyclization, we show that the presence of some residual TFA in the structure may lead to faster reactions in complete agreement with the experiment. Hirshfeld-e partial charges for the Zr ions have been computed to investigate their sensitivity to substituent effects; a strong correlation with the experimental Hammett parameters and with the rates of the citronellal cyclization is found. The theoretical rationalization may serve as a basis for detailed active site engineering studies.

Received 12th August 2014,
Accepted 12th September 2014

DOI: 10.1039/c4ce01672f

www.rsc.org/crystengcomm

Introduction

Metal–organic frameworks (MOFs) are part of a class of hybrid materials. They are porous crystals, composed of interconnecting inorganic and organic moieties.[1–4] Due to their unparalleled porosity and because of the similarity with zeolites and other porous catalysts, MOFs were initially assumed to have potential as catalysts for a wide range of reactions.[5–11] Stability issues (thermal, chemical and mechanical) severely limit the possible industrial applications of many MOFs. The UiO-66 type materials display high thermal stability and retain their crystal structure under relatively extreme conditions. They fulfil the high requirements needed to be useful in commercial applications.[12–14] They are typically composed of inorganic $[Zr_6O_4(OH)_4]^{12+}$ bricks and terephthalate linkers forming a coordinatively saturated framework with eightfold coordination of Zr. Surprisingly, the UiO materials showed catalytic activity,[15] which was ascribed to missing linkers in the structure.[16,17] Similarly, missing terephthalate linkers were also needed to explain the catalytic activity of the vanadium MOF MIL-47 for the epoxidation of cyclohexene.[18,19] An increase in the observed catalytic activity is, in most cases, due to the creation of a larger number of active sites or due to modulating effects resulting from functionalization of the linkers. It has been demonstrated that UiO-66 materials synthesized from terephthalates substituted with electron-withdrawing groups are significantly more active.[17] Many other isoreticular UiO materials have been made with different organic linkers,[13,14,20–27] making use of different protocols including post-synthetic functionalization,[26,28–32] post-synthetic substitution of Zr^{4+}

[a] *Center for Molecular Modeling, Universiteit Gent, Technologiepark 903, B-9052 Zwijnaarde, Belgium. E-mail: Matthias.Vandichel@Ugent.be*
[b] *Centre for Surface Chemistry and Catalysis, Universiteit Leuven, Arenbergpark 23, B-3001 Leuven, Belgium*

† Electronic supplementary information (ESI) available. See DOI: 10.1039/c4ce01672f

cations,[33,34] impregnation with metal nanoparticles,[35–39] *etc.* This shows the great versatility of UiO-66 type materials, with many possible industrial catalytic applications ahead.

As missing linkers create open Zr sites which are accessible for catalytic transformations, procedures were developed to increase these structural defects within the UiO-66 type materials by varying the modulator concentration,[40–42] synthesis time[40] and synthesis temperature.[43] Vermoortele *et al.*[41] demonstrated how a correct use of monocarboxylic modulators, such as trifluoroacetic acid (TFA) in combination with hydrochloric acid (HCl), leads to more active sites within the UiO-66 after a post-synthesis treatment under vacuum at an elevated temperature.[41] The main conclusions can be summarized as follows: (i) TFA does not affect the crystallinity nor the crystal size; (ii) TFA increases the activity for several Lewis acid catalysed reactions; (iii) thermal treatment of the material leads not only to dehydroxylation of the Zr bricks but also to post-synthetic removal of TFA, creating more open metal sites; (iv) a combined use of TFA and HCl during the synthesis even increases the activity of the TFA-modulated material.

The UiO-66 material is an optimal test case for a theoretical study in an attempt to elucidate the underlying mechanism of modulation, as the material shows the unusual phenomenon to exhibit a significant amount of missing linker defects, as reported by many other authors. Wu *et al.* have shown that the amount of missing linkers can be tuned systematically by increasing the concentration of the acetic acid modulator and the synthesis time.[40] In contrast to what has been observed in the case of TFA, other modulators such as acetic acid and benzoic acid increase the crystallinity and particle size of the UiO-66.[44] Recently, replacing BDC by benzene-1,3,5-tricarboxylic acid (BTC) in a synthesis using monocarboxylic acids resulted in structures with even larger pore sizes.[45,46] Especially, MOF-808 (ref. 45) has great opportunities in catalysis, *e.g.* after a thermal activation, all Zr sites become accessible for catalytic transformations.

The role of addition of HCl to the reaction mixture forms an interesting item in the whole synthesis process too, but its influence is not straightforward and strongly dependent on the other synthesis conditions. It greatly accelerates the synthesis of UiO-66 materials without loss of crystallinity or porosity.[47,48] However, the crystallization is slower than upon addition of water, due to the protonation of the linker under strongly acidic conditions.[48]

The effect of synthesis temperature and linker concentration on the thermal stability and defectivity of UiO-66 has also been investigated by the Oslo group.[43] They prepared an almost defect-free material when the synthesis temperature is increased to 220 °C together with an increased linker concentration using a BDC : Zr molar ratio of 2.1.

In the search for MOFs containing correlated defect nanoregions allowing a controlled design of complex active sites for targeted catalysis, the recent work of Cliffe *et al.* is truly inspiring.[49] They replaced Zr by Hf to fabricate UiO-66(Hf),[50] belonging to the same isoreticular family, and found that correlations between cluster defects – *i.e.* missing $Hf_6O_4(OH)_4(BDC)_{12}$ parts in the framework – can in fact be introduced and controlled, offering a lot of new perspectives. However, this new MOF falls outside the scope of the present study and will not be investigated. Defect engineering in MOFs becomes more and more actual and not restricted to UiO materials. Defect-engineered variants of $[Ru_3(btc)_2Cl_{1.5}]$ compounds have been recently synthesized with multifunctional properties ranging from hydrogenation to oxidation and Lewis acid catalysis.[51] In the same spirit of engineering of structural defects, we refer to the work of Farrusseng and coworkers.[52]

Molecular modelling can serve as a complementary tool to find a plausible explanation for the abovementioned features. One of the main objectives of this paper is to gain a greater understanding of the chemical transformations of the UiO-66 type materials during the synthesis and post-synthesis processes under real operating conditions. To the best of our knowledge, such theoretical calculations have not yet been performed up to now. They open a lot of perspectives in particular when the applied methodology turns out to be successful in reproducing the main features occurring in the synthesis and post-synthesis processes of UiO-66 when tuning the various synthesis degrees of freedom. The thus obtained knowledge can be regarded as a breakthrough toward active site engineering in MOFs by intentional creation of defects.

All modified synthesis procedures result in many missing linkers, as expressed in the larger pore size distribution, elemental analysis or TGA.[16,17,41,47,53]

An in-depth theoretical rationalization of the mechanisms governing the defect creation is very challenging and various aspects need to be taken into account. The first issue concerns the defect creation during synthesis and how it can be tuned by adding modulators (TFA, HCl, H_2O) to the reaction mixture under specific reaction conditions, such as temperature and concentrations of the different ingredients. The second issue deals with thermal activation during a post-synthetic process and the removal of different compounds, such as intra-framework bound water and TFA. These processes are very competitive and will be subjected to a thorough investigation. Further, a lot of attention is drawn to the dehydroxylation of the inorganic brick. In this work, a dehydroxylation pathway will be proposed, which is not straightforward and which results from a rather complex two-step procedure. First, molecular dynamics techniques have been applied to explore the free energy surface and to identify plausible pathways. In a second step, the detected intermediate species are further investigated in combination with the nudged elastic band[54,55] (NEB) method to reveal the minimum energy pathways between them. The NEB method was also previously used on MOFs to investigate the structural transformations of COMOC-2.[56] Finally, different engineered active site models are studied for catalysis and attempts are made to correlate partial Hirshfeld-e[57] charges of the exposed Zr sites with the catalytic activity.

 This journal is © The Royal Society of Chemistry 2014

In the remaining parts of the paper, we focus on the computational results rather than on the methodology. We refer to the ESI† for further details and a summary of all investigated species and links between them under synthesis and activation conditions (Fig. S4 and S5†).‡

Results and discussion

A. Defect creation during synthesis of UiO-66

A.1 Replacement of linkers by trifluoroacetate (TFA), chloride or hydroxide. In UiO-66 synthesis, 1,4-benzenedicarboxylates (BDCs) are typically incorporated as organic linkers. In a defect-free cubic Zr-terephthalate UiO-66 material, each $Zr_6O_4(OH)_4$ octahedron is surrounded by 12 terephthalate linkers, resulting in large octahedral and small tetrahedral cages. However, under certain synthesis conditions, linker deficiencies may arise and active materials for catalysis were found to have, on average, only 8 carboxylates surrounding the cluster.[41] In the literature,[16,41] in-depth discussions with experimental rationalizations were devoted to the question on whether linker removal occurs in an ordered way. These deficiencies can vary between the complete loss of a terephthalate linker and the replacement of BDC by one of the modulators present in the reaction mixture. These species may coordinate on the inorganic $[Zr_6O_4(OH)_4]^{12+}$ brick. Herein, we present a free energy discussion of various plausible structures and it is anticipated that some structures have a larger probability to occur than others. For theoretical calculations, we assume that besides the BDC linkers TFA and HCl modulators and H_2O are also available in the reaction mixture. If we concentrate on one linker deficiency per unit cell, many combinations are possible. For the sake of transparency in the discussion, each possible synthesis product is represented by a shorthand notation, as outlined in Table 1. We calculated the free energy of formation for all of the possible structures with respect to the defect-free reference state A (X(BDC), Fig. 1). To guarantee mass balance, a pool of isolated molecules is introduced, taking up the removed linker/substituent and withdrawing those molecules from the pool needed to form the new structures. In the calculations, all isolated pool molecules are treated in the gas phase.

All possible synthesis products X(L) are visualized in Fig. 1 with indication of the free energy differences under synthesis conditions of T = 130 °C and p = 1 bar. A complete removal of a terephthalate linker (structure G) requires 300 kJ mol^{-1} and is unlikely to occur. However, the formation of several other defect structures requires a lower free energy. The presence of TFA as a modulator yields structures which are energetically reachable. The formation of structure C with two TFA groups coordinated at the metal in the space left by the removal of a BDC linker only requires 85.9 kJ mol^{-1}. The probability of formation of such a structure can be significantly increased by enlarging the TFA/BDC ratio in the reaction mixture. This is exactly what is observed experimentally.[41] Note that no solvent effects were included in our calculations, especially for structures with open Zr sites, inclusion of explicit solvent molecules would most probably result in an additional stabilization of these structures with respect to X(BDC). However, solvent effects will not qualitatively change the results displayed in Fig. 1. Remark that a description of solvent effects is not straightforward as the synthesis mixture consists of many different species, which are able to coordinate with open metal sites.

Despite the fact that the fully saturated structure A (X(BDC)) is by far the thermodynamically most stable structure, it is not excluded that also other linker deficiencies can occur and that their probability grows with increasing excess of H_2O, HCl, TFA or any other modulator with respect to the dicarboxylate linker.[41] In principle, this excess – in combination with well-chosen synthesis parameters such as temperature[43] and synthesis time[58] – may lead to defect sites which are displayed in Fig. 1.

Some defect structures are less probable. The incorporation of hydroxyl groups requires a free energy of 240.2 kJ mol^{-1} under synthesis conditions.

The decomposition of the free energy into enthalpic and entropic contributions can shed insight into the underlying reasons why some defect deficiencies occur with larger probability than others (see Table 2). The enthalpic penalty of 393.1 kJ mol^{-1} corresponding to the removal of a terephthalate linker (C → G) is hardly compensated by the entropy gain. This large value can also be interpreted as a large stabilization induced by the coordination of two carboxyl groups. Starting from structure G (X(0)) with four uncoordinated Zr sites, any coordination with the metal yields extra stabilization which is clearly visible in Fig. 1. This stabilization can vary a lot, but it is significantly larger when all open Zr sites are coordinated. This is best illustrated with the double TFA incorporation showing a reaction enthalpy of −385.8 kJ mol^{-1} (with respect to G (X(0)) which is of the same order as restoring the defect site with a terephthalate linker. The difference between X(BDC) and X(2TFA) lies mainly in the entropic contribution which is much higher in the latter (compare +171.7 kJ mol^{-1} and +92.6 kJ mol^{-1} (relative with respect to X(0) (Table 2)). In reality, the enthalpy barriers may be somewhat reduced as all isolated molecules which are removed are treated in the gas phase here but, under circumstances of synthesis, will also be stabilized to some extent by the molecular environment of the reaction mixture. In any case, the breakage of the inorganic–organic linkage is the main source for the large enthalpy penalties observed here.

Besides trifluoroacetate incorporation, chloride incorporation and hydroxide incorporation, starting from HCl and water, respectively, were also considered. Incorporation of

‡ Remark that within the fully saturated inorganic brick $Zr_6O_4(OH)_4$, there are two possibilities of hydrogen orientation (*cf.* Fig. S1 and S2†). In all our calculations, we have opted for the tetrahedral orientation given in Fig. S1,† because this arrangement corresponds with the lowest energy configuration.[40,53] In the presented reaction schemes, BDC is replaced by two RCOO groups. When using the abbreviations TFA and BDC, we mostly refer to the protonated – *i.e.* charge neutral – molecules.

Table 1 Summary of the notation of the different structures formed during synthesis and post-synthesis treatment. In the Y-structures, Cl^- is incorporated into the inorganic part of the framework. For convenience, the notation $RCOO^-$ is introduced representing half a BDC^{2-} linker, and TFA in the formulas should be read as CF_3COO^-

	Shorthand notation	Unit cell formula	Changes with respect to reference structure
A	X(BDC)	$\langle Zr_6O_4(OH)_4(RCOO)_{12}\rangle_4$	Reference structure without any defect
B	X(TFA)	$\langle Zr_6O_4(OH)_4(RCOO)_{11}(TFA)\rangle$ $\langle Zr_6O_5(OH)_3(RCOO)_{11}\rangle$ $\langle Zr_6O_4(OH)_4(RCOO)_{12}\rangle_2$	BDC → TFA
C	X(2TFA)	$\langle Zr_6O_4(OH)_4(RCOO)_{11}(TFA)\rangle_2$ $\langle Zr_6O_4(OH)_4(RCOO)_{12}\rangle_2$	BDC → 2TFA
D	X($2H_2O$)	$\langle Zr_6O_4(OH)_4(RCOO)_{11}(OH)\rangle_2$ $\langle Zr_6O_4(OH)_4(RCOO)_{12}\rangle_2$	BDC → $2H_2O$
E	X(2HCl)	$\langle Zr_6O_4(OH)_4(RCOO)_{11}(Cl)\rangle_2$ $\langle Zr_6O_4(OH)_4(RCOO)_{12}\rangle_2$	BDC → 2HCl
F	$X^{H_2O\uparrow}$(BDC)	$\langle Zr_6O_5(OH)_2(RCOO)_{12}\rangle$ $\langle Zr_6O_4(OH)_4(RCOO)_{12}\rangle_3$	Removal of one H_2O from one Zr_6 brick
G	X(0)	$\langle Zr_6O_5(OH)_3(RCOO)_{11}\rangle_2$ $\langle Zr_6O_4(OH)_4(RCOO)_{12}\rangle_2$	Removal of one BDC linker
H	$X^{H_2O\uparrow}$(TFA)	$\langle Zr_6O_5(OH)_2(RCOO)_{11}(TFA)\rangle$ $\langle Zr_6O_5(OH)_3(RCOO)_{11}\rangle$ $\langle Zr_6O_4(OH)_4(RCOO)_{12}\rangle_2$	Removal of one H_2O from one Zr_6 brick and BDC → TFA
I	$X^{2H_2O\uparrow}$(BDC)	$\langle Zr_6O_6(RCOO)_{12}\rangle$ $\langle Zr_6O_4(OH)_4(RCOO)_{12}\rangle_3$	Removal of two H_2O from one Zr_6 brick
J	$X^{2H_2O\uparrow}$(TFA)	$\langle Zr_6O_6(RCOO)_{11}(TFA)\rangle$ $\langle Zr_6O_5(OH)_3(RCOO)_{11}\rangle$ $\langle Zr_6O_4(OH)_4(RCOO)_{12}\rangle_2$	Removal of two H_2O from one Zr_6 brick and BDC → TFA
K	$X^{H_2O\uparrow}$(0)	$\langle Zr_6O_6(OH)\,(RCOO)_{11}\rangle$ $\langle Zr_6O_5(OH)_3(RCOO)_{11}\rangle$ $\langle Zr_6O_4(OH)_4(RCOO)_{12}\rangle_2$	Removal of one H_2O from one Zr_6 brick and removal of one BDC linker
L	Y(BDC)	$\langle Zr_6O_4Cl(OH)_3(RCOO)_{12}\rangle_2$ $\langle Zr_6O_4(OH)_4(RCOO)_{12}\rangle_2$	Incorporation of Cl^- in two Zr_6 bricks of the reference structure (OH^- → Cl^- in two bricks)
M	Y($2H_2O$)	$\langle Zr_6O_4Cl(OH)_3(RCOO)_{11}(OH)\rangle_2$ $\langle Zr_6O_4(OH)_4(RCOO)_{12}\rangle_2$	Rearrangement of X(2HCl) by incorporating Cl^- into the cluster
N	X(TFA,HCl)	$\langle Zr_6O_4(OH)_4(RCOO)_{11}(TFA)\rangle$ $\langle Zr_6O_4(OH)_4(RCOO)_{11}(Cl)\rangle$ $\langle Zr_6O_4(OH)_4(RCOO)_{12}\rangle_2$	BDC → TFA and HCl
O	$Y^{2H_2O\uparrow\ 2HCl\downarrow}$ (2HCl)	$\langle Zr_6O_4Cl(OH)_3(RCOO)_{11}(Cl)\rangle_2$ $\langle Zr_6O_4(OH)_4(RCOO)_{12}\rangle_2$	Incorporation of Cl^- in two Zr_6 bricks of the reference structure and replacement of two coordinating OH^- groups by Cl^-

This journal is © The Royal Society of Chemistry 2014

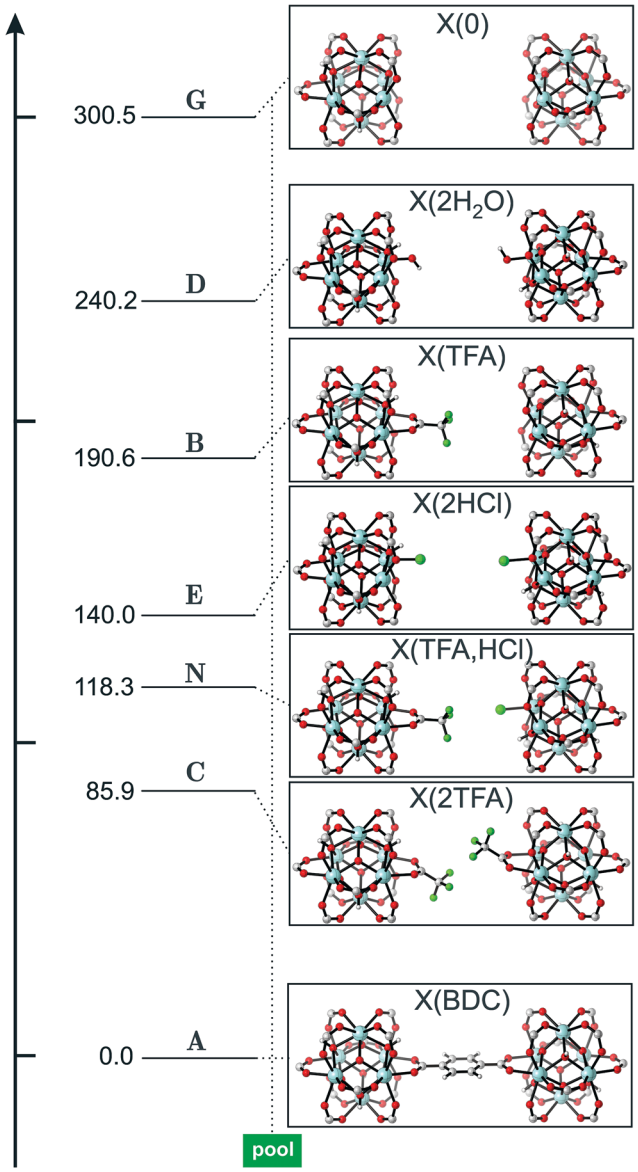

Fig. 1 Different linker replacements X(L) which take place during the synthesis of UiO-66 with BDC, TFA, HCl and H_2O in the reaction mixture. Free energy differences in kJ mol^{-1} are reported with respect to the reference configuration A during synthesis conditions (T = 130 °C, p = 1 bar). A pool with isolated linkers and modulators in gas phase is added to guarantee mass balance in the equilibrium reactions. The results were obtained in a periodic calculation with the PBE-D3(BJ) functional, employing an energy cutoff of 400 eV.

chloride (structure E (X(2HCl)) is clearly favoured over water incorporation (structure D (X($2H_2O$)), with reaction free energy differences of −160.5 and −60.3 kJ mol^{-1}, respectively, but a combined structure X(TFA,HCl) yields an even larger stabilization energy (−182.2 kJ mol^{-1}).

Summarizing, while linker deficiencies arise during the synthesis, their formation is certainly not thermodynamically preferred. However, the introduction of modulators such as TFA considerably reduces the free energy barrier for formation of linker deficiencies. It may be anticipated that defect formation is a kinetic process which is also highly dependent on synthesis temperature, synthesis time and modulator concentrations. TFA is a modulator competing best with the BDC linkers, which is evidenced by the energy calculations, and which is also observed experimentally when increasing the TFA : BDC ratio in the synthesis.[41] Similarly, chloride incorporation becomes more likely at high HCl/TFA ratios.

Table 2 Free energies and their enthalpic and entropic contributions for the formation of defect structures with respect to the defect-free reference site A (X(BDC)) under synthesis conditions (T = 130 °C, p = 1 bar). All energies are given in units of kJ mol^{-1}. The results were obtained with the PBE-D3(BJ) functional, employing an energy cutoff of 400 eV

		ΔG	ΔH	$-T \cdot \Delta S$
A	X(BDC)	0.0	0.0	0.0
C	X(2TFA)	85.9	6.9	79.1
N	X(TFA,HCl)	118.3	68.3	49.9
E	X(2HCl)	140.0	117.9	22.1
B	X(TFA)	190.6	199.0	−8.4
D	X($2H_2O$)	240.2	215.9	24.3
G	X(0)	300.5	393.1	−92.6

A.2 Incorporation of chlorine in the inorganic $Zr_6O_4(OH)_4$ bricks. Chlorides in the reaction mixture, either arising from $ZrCl_4$ or from added HCl, can be incorporated in the framework in the following two ways: (i) the Cl^- anions can peripherally coordinate to the $[Zr_6O_4(OH)_4]^{12+}$ cluster by replacing a BDC linker (structure X(2HCl); see section A.1), and (ii) the Cl^- anion can be incorporated into the cluster itself by replacing OH^- groups (structures Y(BDC) and Y(2HCl)) (Fig. 2). The latter modification has been proposed very recently by Lillerud *et al.*[53] who detected Cl^- residues within some of their synthesized UiO-66 materials, originating from the Zr precursor $ZrCl_4$. They postulated that the chloride might substitute the μ_3-OH groups on the cluster (structure L (Y(BDC)) in Fig. 2a). This is indeed possible, as Cl^- is present in the $ZrCl_4$ and $ZrOCl_2$ precursors that are typically used or can be added in the form of HCl.[47,48] If HCl is added during the synthesis, Cl^- anions were also found in the materials by elemental analysis.[47]

The incorporation of chloride is theoretically quite feasible, as the Gibbs free energy (ΔG) for the reaction A + 2HCl → L + $2H_2O$ amounts to −3.4 kJ mol^{-1} at 130 °C (Fig. 2a). Energetically Y(BDC) is even more stable than the standard defect-free X(BDC) structure, but there is an entropic penalty which compensates the enthalpic release of 53.8 kJ mol^{-1} at a temperature of about 157 °C and which will become dominant at higher synthesis temperatures. Under such conditions, Cl^- incorporation is no longer favoured, which is in perfect agreement with the procedure for synthesizing a pure Cl-free UiO-66 at 220 °C applied by Shearer *et al.*;[43] as for this UiO-66, no chlorine was found after 2 DMF washes, and Cl^- was not incorporated in the inorganic brick during synthesis. This is in sharp contrast with the same material, which has been synthesized at 100 °C by the same authors, but where the Cl^- could not have been washed out by DMF (see Table S4 of ref. 43).

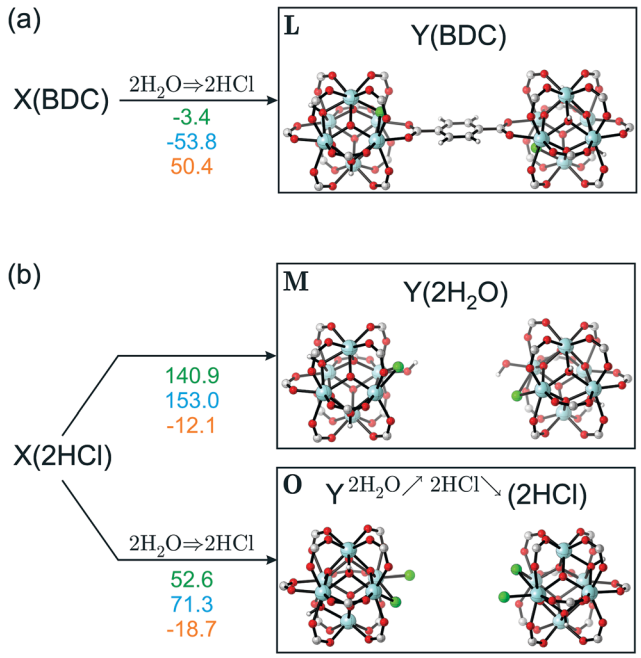

Fig. 2 (a and b) Free energy differences (green) with respect to the reference X(BDC) structure in (a) and X(2HCl) in (b) for the incorporation of Cl^- in the frame during synthesis (T = 130 °C, p = 1 bar). The enthalpic (blue) and entropic (orange) contributions are also given. The energies are given in units of kJ mol^{-1}. The results were obtained with the PBE-D3(BJ) functional, employing an energy cutoff of 400 eV.

On the other hand, Cl^- can also compensate linker deficiencies, as in structure E (X(2HCl)). In principle, one can consider a migration of a chloride ion from a position outside the cluster (extra-framework Cl^-) to a position inside the cluster, such as the transformation X(2HCl) → Y($2H_2O$) visualized in Fig. 2b. On the basis of energetic considerations, the incorporation of Cl^- in the cluster is however highly inhibited as the Gibbs free energy difference amounts to +140.9 kJ mol^{-1}. This is not in contradiction with experimental findings. Indeed, one can easily expect that the chlorine that is only coordinated with the Zr bricks is easier washed away by DMF, as has been observed in the synthesis of UiO-66 at 100 °C by the Oslo group.[43] Extra-framework Cl^- will also be easily removed by a post-synthesis treatment (Table 3), but this will be discussed in the next session. In Fig. 2b, another route for incorporation of Cl^- within the inorganic brick during synthesis at 130 °C is presented, but the formed structure O is also unlikely to be formed (ΔG = 58.9 kJ mol^{-1}).

Concluding, Cl^- incorporation within the inorganic $[Zr_6O_4(OH)_4]^{12+}$ brick, with formation of $[Zr_6O_4Cl(OH)_3]^{12+}$, is expected to happen at low synthesis temperatures, which was also observed experimentally.[43]

Table 3 Creation of defect sites under activation conditions (T = 320 °C, p = 10^{-3} mbar) from all synthesis structures displayed in Fig. 1. The results were obtained with the PBE-D3(BJ) functional, employing an energy cutoff of 400 eV

	ΔG_r	ΔH_r	$-T \cdot \Delta S_r$
X(BDC) → X(0) + BDC	189.2	390.4	−201.2
X(TFA) → X(0) + TFA	2.6	191.3	−188.7
X(2TFA) → X(0) + 2TFA	−1.4	380.3	−381.7
X($2H_2O$) → X(0) + $2H_2O$	−130.0	171.5	−301.5
X(2HCl) → X(0) + 2HCl	−29.3	272.3	−301.6
X(TFA,HCl) → X(TFA) + HCl	−23.0	129.2	−152.2
X(TFA,HCl) → X(0) + HCl + TFA	−20.4	320.5	−340.8

B. Thermal activation or post-synthesis activation

In the previous subsection, the most probable synthesis products have been discussed with a variety of defect structures under synthesis conditions of the material (T = 130 °C, p = 1 bar). For use of the materials as catalysts, the as-synthesized materials are activated by a post-synthesis procedure to create open metal sites. The processes during thermal activation are discussed in the following two sections. A complete overview of the investigated species and reactions between them is given in the ESI† (Fig. S4 and S5).

B.1 Creation of active, uncoordinated Zr sites by thermal removal of coordinating species. Vermoortele *et al.*[41] have shown that thermal activation of the trifluoroacetate (TFA) substituted UiO-66 leads not only to dehydroxylation of the hexanuclear $[Zr_6O_4(OH)_4]^{12+}$ cluster but also to post-synthetic removal of the TFA groups. These processes result in a more open framework with a large number of open sites and consequently a higher catalytic activity for Lewis acid catalyzed reactions. In this paper, the post-synthesis activation treatment was modelled under the conditions T = 320 °C and p = 10^{-3} mbar starting from the structures displayed in Fig. 1 (Table 3).

The higher temperature with respect to the synthesis conditions results in defect formation processes that are more entropy driven. This could be anticipated from the entropy contributions in the formation of various defect structures in the previous section (Table 2). The fully coordinated UiO-66 structure X(BDC) will still not undergo a deterephthalation (direct removal of terephthalic acid or BDC) as the free reaction energy of 189.2 kJ mol^{-1} (Table 3) is too high. This process will not occur during the synthesis or the post-synthesis treatment without the destruction of the linker.[16] Additionally, the removal of TFA from all structures in which TFA is coordinated to the zirconium is very probable, in view of the low or even generally negative free energies for all these processes (see Table 3). This is in sharp contrast with the BDC removal from structure X(BDC): 189.2 kJ mol^{-1} *versus* −1.4 kJ mol^{-1} for the removal of the two coordinated TFA molecules in X(2TFA). This feature is highly remarkable as the two structures show similar large enthalpy stabilization effects under synthesis conditions (Fig. 1). It is the entropy term which at 320 °C becomes sufficiently large to compensate the enthalpic stabilization (Table 3).

Another phenomenon becomes important under thermal activation conditions: dehydroxylation of the material becomes competitive with TFA withdrawal. To illustrate this,

 This journal is © The Royal Society of Chemistry 2014

we start from the formed X(TFA) structure and investigate the free energy change associated with water or TFA removal under post-synthetic conditions (Fig. 3). A partial dehydroxylation is thermodynamically even more favourable (free energy difference of −55.6 kJ mol^{-1}). Such partial dehydroxylation is then followed by TFA removal or another dehydroxylation. Both steps are in competition, in view of reaction free energies of the order of −25 kJ mol^{-1} (see Fig. S5 of the ESI†).

It should be noted that in the case of UiO-66–NO_2, not all TFA molecules could be removed by a post-synthesis treatment,[41] by the simple reason that the temperature needed to remove TFA just coincides with the decomposition temperature of the material.

If linker deficiencies coordinated with hydroxide or chloride ions at the periphery of the cluster are present in the framework after synthesis (*e.g.* structure X(2HCl) or X(2H_2O)), a thermal activation will remove all these molecules with reaction free energy differences of −65.0 kJ mol^{-1} (per H_2O molecule) and −14.7 kJ mol^{-1} (per HCl molecule) (Table 3).

B.2 Mechanism of the dehydroxylation processes of inorganic $Zr_6O_4(OH)_4$ bricks. In the lowest energy configuration, hydrogen atoms of hydroxyl groups are expected to be ordered in a tetrahedral fashion in the inorganic bricks (Fig. S1†). To unravel the dehydroxylation processes and the intermediate structures involved, we applied a two-step procedure. First, we explored the free energy surface by performing an NPT simulation of our model system at a pressure of 10^{-9} bar with already one terephthalate linker missing in the structure (for further computational details, see ESI†). The temperature was increased step by step (100 K per 2 ps) to enhance the dehydroxylation process. At a certain temperature (1273 K), we observed the simultaneous decoordination of a μ_3-OH group and one of the three neighbouring terephthalates. Based on this simulation, a decoordinated state was constructed for the small model system (with two Zr bricks in a unit cell) and further optimized (structure 18 as given in the ESI†). With one missing BDC linker, the formula becomes $<Zr_6O_4(OH)_4(RCOO)_{12}Zr_6O_6(OH)_2(RCOO)_{10}>$. The two Zr bricks are displayed in Fig. 5. We investigate the dehydroxylation of brick 1 as initial unperturbed structure 0 (Fig. 4).

Inspired by this decoordinated state observed during the NPT simulations, we performed a series of nudged elastic band (NEB) simulations[54,55] between the initial structure 0 and end structure 27 in order to fully construct the electronic profile associated with the dehydroxylation along pathway 1. The resulting profile is given in Fig. 4. A maximum is encountered at structure 7, which corresponds to a structure in which one carboxylic group is partially decoordinated from the Zr atom and in which the hydroxyl group is also detached from the Zr atom. After that, some

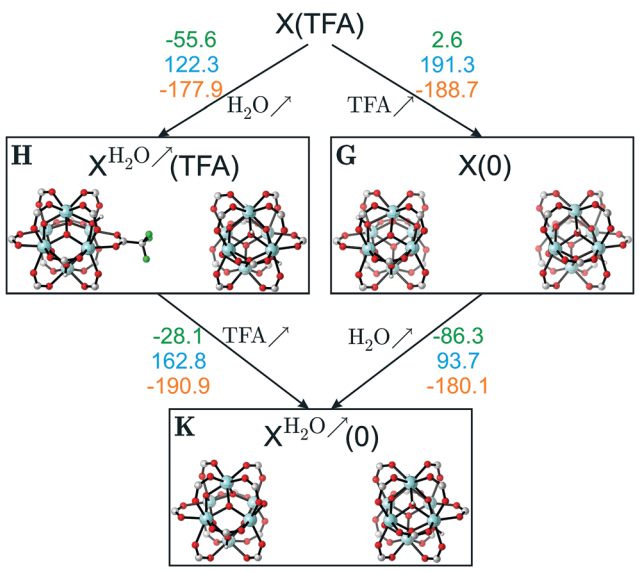

Fig. 3 Water *versus* TFA removal from structure X(TFA) under post-synthesis activation conditions (T = 320 °C and p = 10^{-3} mbar). Free energy differences (green) and enthalpic (blue) and entropic (orange) contributions are also given. The results were obtained with the PBE-D3(BJ) functional, employing an energy cutoff of 400 eV.

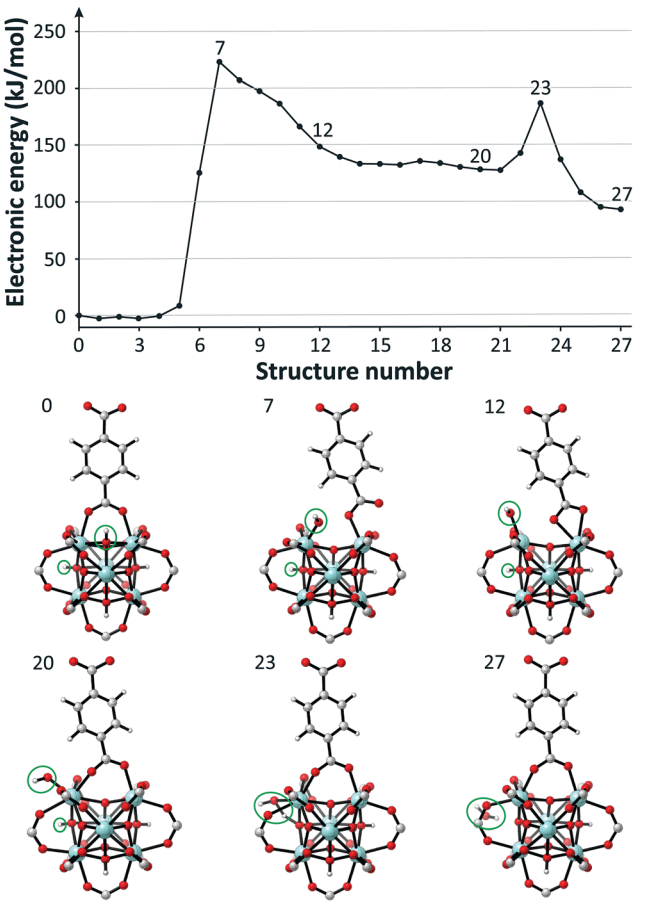

Fig. 4 Electronic energy profile for the first dehydroxylation reaction. The relevant atoms leading to the final removal of water are encircled. The linkers, which are not involved in the dehydroxylation, are not displayed. The electronic energies were obtained from an energy refinement (on all the images) with the PBE-D3(BJ) functional, employing an energy cutoff of 400 eV.

intermediate structures are observed where the linker coordinates to the same Zr atom (structure 12) and afterwards coordinates back to the two Zr sites (structure 20). Structure 20 is an energetic minimum on the potential energy surface, and at that moment, the hydroxyl group is in the right position to allow the coordination of the linker with two Zr atoms.

The released hydroxyl will react further by abstracting a proton of another available μ_3-OH group (structure 23), followed by the release of a water molecule (structure 27).

The process of dehydroxylation is also schematically shown in Fig. 5. After water removal, the unit cell formula contains two inorganic bricks with two hydroxyl groups each (formula: $<Zr_6O_5(OH)_2(RCOO)_{12}Zr_6O_6(OH)_2(RCOO)_{10}>$). This structure can undergo two additional dehydroxylation reactions (pathways 2 and 3; see Fig. 5) The second dehydroxylation of the $[Zr_6O_4(OH)_4]^{12+}$ brick results in a $[Zr_6O_6]^{12+}$ brick with two neighbouring oxygen defects. One Zr atom is then sixfold coordinated, one is eightfold coordinated and four sevenfold; on the average, this also results in a sevenfold Zr coordination as demonstrated by EXAFS measurements.[16] In the work of Cavka *et al.*,[12] the second dehydroxylation of a fully coordinated structure yields a $[Zr_6O_6]^{12+}$ brick in which each Zr should be threefold coordinated by an oxo-oxygen atom. The $[Zr_6O_6]^{12+}$ brick is thus assumed to have opposite oxygen defects. This looks at first glance in contradiction with Fig. 5. However, in case of neighboring oxygen defects, the dehydroxylated cluster can undergo an oxygen shift to form a brick with two opposite oxygen defects.

Some comments have to be made regarding the dehydroxylation process. First, in the case of a higher number of missing linkers, no dehydroxylation can take place. The dehydroxylation pathways would also change if linker deficiencies are present, as is schematically shown in the bottom of Fig. 5.

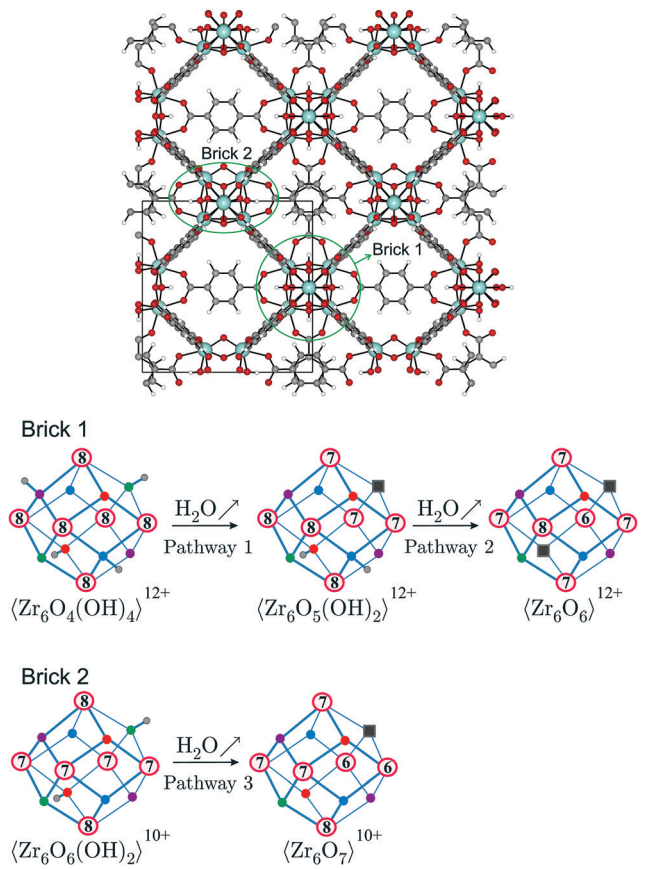

Fig. 5 At the top of the figure, the structure of the modelled UiO-66 crystal is displayed with indication of the unit cell. Zr-brick 1 with formula $<Zr_6O_4(OH)_4(RCOO)_{12}>$ is intact with no missing linker, while brick 2 $<Zr_6O_6(OH)_2(RCOO)_{10}>$ has one missing terephthalate linker. Dehydroxylation processes can start from brick 1 and from brick 2. Coordination numbers of the different Zr atoms in the brick are given (encircled). Oxygen vacancies are displayed as grey squares.

C. Linker deficiencies and their role in the catalytic activity

The catalytic activity of the UiO-66 material has already been investigated by the authors in a combined experimental–theoretical work.[17,41] The citronellal cyclization was taken as a model reaction, as both activity and selectivity for the isopulegol isomers were strongly dependent on the Lewis acidity of the active site. However, there are many factors governing the experimentally measured activity, making a direct comparison with theory very challenging. The activity depends on (i) the number of active sites that effectively take part in the reaction and (ii) the Lewis acid strength, intrinsically responsible for the reaction rate of a single event. This excludes a direct quantitative comparison of the measured citronellal conversion with theory. What theory should, in principle, be able to reproduce is the relative increase/decrease of the observed conversion by electronic effects. We demonstrated that some specific functionalizations of the linkers of the UiO-66 material can significantly increase the catalytic activity for the citronellal cyclization. For example, nitro-substituted UiO-66 (UiO-66–NO_2) resulted in an experimental 56-fold increase of the reaction rate, which could be qualitatively reproduced by theoretical modelling.[17] Hereto, extended cluster models have been systematically applied, and despite their inadequacy to fully take the environment into account, they have shown their merits in the description of single reaction events and in the qualitative prediction of the reaction rate constants. To obtain preliminary insight into the modulation effects of TFA, HCl, *etc.*, on the reactivity, an extended cluster approach was also used in this paper. For reference purposes, we choose to model the reaction rate constant for the citronellal cyclization which has been thoroughly tested experimentally.

We examined the role of the linker deficiencies with traces of TFA coordinated to the metal site. In a recent work of the authors,[41] it is found that the addition of small quantities of TFA to the synthesis already significantly increases the activity, although a maximum activity is obtained when adding 20 equiv. of TFA. This is a serious indication that the increase of activity is due to the creation of a larger number of open sites rather than to a modified acid strength. To verify this,

 This journal is © The Royal Society of Chemistry 2014

we constructed extended clusters with trifluoroacetic acid (TFA) (see Fig. S7†), in which we varied the TFA position to evaluate whether TFA has a stronger influence if it is in the immediate surroundings of the active Zr site. Two terephthalate linkers, closest to the active site, are maintained in the cluster. The other linkers are replaced by formate groups. One of them is replaced by TFA.

Despite the assumptions made in the model space, the results are able to give a first impression on the extent to which the citronellal cyclization activity varies between the UiO-66 and UiO-66/TFA models (and UiO-66–NO_2 and UiO-66–NO_2/TFA models, respectively). All kinetic data are summarized in Table 4. The apparent kinetic data are based on gas phase reactants, while the intrinsic data are determined from the adsorbed reactants. We also rely on the concerted character of the citronellal cyclization on Lewis acid catalysts, as was proposed in earlier studies.[17,59]

The presence of a TFA group in the cluster model results in a stronger adsorption enthalpy of the reactant which generally leads to more stable adsorption free energies for the reactant, transition and product states relative to the clusters without TFA insertion. On average, the TFA group does not change the intrinsic or apparent entropy contribution to the free energy.

Relative to the UiO-66 model, the apparent rate acceleration of the modified models is systematically higher than the intrinsic rate acceleration. The electronic modulation effect of the nitro linker functionalization is even more pronounced with the presence of the TFA modulator. This theoretical result confirms what has been observed experimentally,[41]

Table 4 Kinetic data for the citronellal cyclization to isopulegol at 373 K (clusters in Fig. S6). Free energy, enthalpy and entropy contributions in the adsorbed state (ads) and in the transition state (‡) (kJ mol^{-1}). The rate constants (k_{373}^{fwd}) are given in units of m^3 mol^{-1} s^{-1} for the apparent kinetics and in s^{-1} for the intrinsic kinetics. The relative rates *versus* the non-modulated UiO-66 material are also given in brackets

Pre-TS	ΔG_{373}^{ads}	ΔH_{373}^{ads}	$-T \cdot \Delta S_{373}^{ads}$	
UiO-66[a]	−15.7	−88.6	72.9	
UiO-66/TFA1	−19.4	−93.0	73.6	
UiO-66/TFA2	−18.7	−92.2	73.5	
UiO-66–NO_2[a]	−23.7	−104	80.4	
UiO-66–NO_2/TFA1	−30.3	−109.6	79.3	
UiO-66–NO_2/TFA2	−26.6	−107.5	80.8	
Apparent	$\Delta G_{373}^{‡}$	$\Delta H_{373}^{‡}$	$-T \cdot \Delta S_{373}^{‡}$	k_{373}^{fwd}
UiO-66[a]	56.4	−44.2	100.6	3.03×10^3 (1.0)
UiO-66/TFA1	51.5	−49.2	100.6	1.49×10^4 (4.9)
UiO-66/TFA2	52.0	−49.1	101.1	1.24×10^4 (4.1)
UiO-66–NO_2[a]	37.4	−67.8	105.2	1.40×106 (463.3)
UiO-66–NO_2/TFA1	32.8	−72.8	105.5	6.18×10^6 (2039.1)
UiO-66–NO_2/TFA2	32.1	−71.6	103.7	7.79×10^6 (2572.1)
Intrinsic	$\Delta G_{373}^{‡}$	$\Delta H_{373}^{‡}$	$-T \cdot \Delta S_{373}^{‡}$	k_{373}^{fwd}
UiO-66[a]	72.1	44.4	27.8	6.15×10^2 (1.0)
UiO-66/TFA1	70.9	43.8	27.0	9.28×10^2 (1.5)
UiO-66/TFA2	70.7	43.1	27.6	9.72×10^2 (1.6)
UiO-66–NO_2[a]	61.1	36.4	24.7	2.17×10^4 (35.4)
UiO-66–NO_2/TFA1	63.1	36.8	26.3	1.13×10^4 (18.4)
UiO-66–NO_2/TFA2	58.7	35.8	22.9	4.68×10^4 (76.2)

[a] Data taken from ref. 17

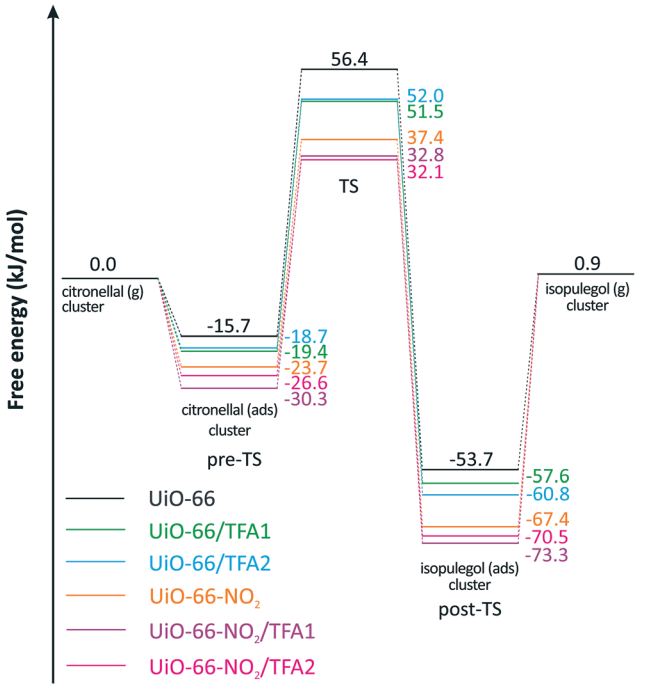

Fig. 6 Free energy profiles, calculated at 373 K, for citronellal cyclization to isopulegol. Results for UiO-66 and UiO-66–NO_2 were adopted from ref. 17

that the more open pore structure and the larger number of open sites, resulting from a combined use of TFA and HCl during the synthesis, strengthen the electronic effect of the nitro group. Free energy profiles are displayed in Fig. 6, clearly showing the order of activity based on the apparent barriers: UiO-66 < UiO-66/TFA < UiO-66–NO_2 < UiO-66–NO_2/TFA.

Note that the employed extended cluster model attains its limits in these applications and that more expensive periodic calculations could give more insight into the influence of the environment. For reactions taking place on adjacent Zr sites, such as the aldol condensation[15] and the Oppenauer oxidation,[17] cluster models are no longer sufficient.

In an attempt to elucidate the different electronic modulation patterns induced by the substituents, we investigated the charge on the open Zr site of the different cluster models in relation to the activation enthalpy for the citronellal cyclization. Of the several charge population schemes, we prefer to choose the recent Hirshfeld-e partitioning scheme[57] as it combines electrostatic potential accuracy with transferability. For a series of functionalized UiO-66–X materials, some of the present authors have previously found a linear free energy relationship (LFER) between the activity in Lewis acid catalysed reactions and the experimental Hammett constant σ_m (ref. 60) as a measure of the electronic nature of the ligands.[17] In this work, we aimed at finding a theoretical criterion which correlated well with the experimental Hammett constants. Within this scope, we calculated the Hirshfeld-e charges of the metal in ten different cluster models (Fig. S10†) and plotted them *versus* σ_m, σ_p and an average combination of them (σ_{avg} = log(10^(σ_p) + 10^(σ_m)), as

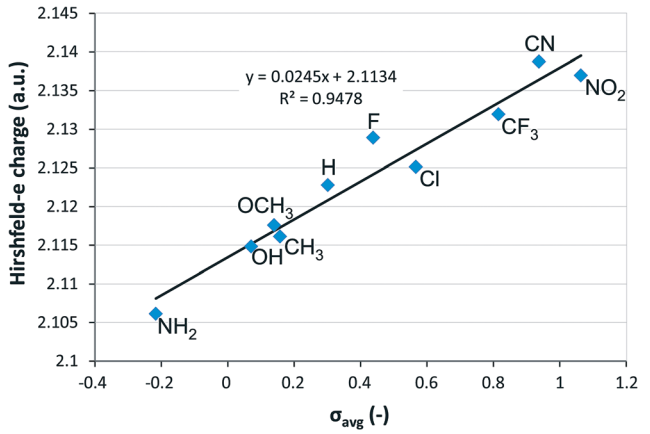

Fig. 7 Hirshfeld-e charge of Zr *versus* an average Hammett constant σ_{avg}. The cluster models are shown in Fig. S10.†

substituents can either be in *ortho* or *meta* position with respect to the active Zr site. For all three Hammett constants, a rather good correlation with the Hirshfeld-e charges was found ($R^2 > 0.85$). Fig. 7 displays the correlation diagram belonging to σ_{avg}, which shows the best agreement. This clear correlation suggests that Zr Hirshfeld-e charges may be regarded as a valid alternative to predict a qualitative indication of the catalytic activity of hypothetical UiO-66–X variants. From the data reported here (Fig. 7), we estimate that UiO-66 with CN or CF_3 substituent groups will have a catalytic activity that is comparable to that of UiO-66–NO_2.

Conclusions

In idealized non-defective UiO-66 type materials, the inorganic $[Zr_6O_4(OH)_4]^{12+}$ bricks are fully coordinated with benzenedicarboxylate (BDC) linkers and the Zr sites are thus inaccessible for catalytic activity. This activity can be switched on if linker deficiencies can be introduced in the material, creating structural coordinatively unsaturated Lewis acid sites. Modulation approaches during the synthesis are experimentally the most prominent and efficient techniques to tune the synthesized product, as the experimentalist freely disposes of a lot of parameters, such as synthesis time, synthesis temperature, nature of the modulators (MDL) and their concentration. In this paper, an attempt is made to elucidate the processes taking place during the synthesis – in particular the role of modulating species trifluoroacetic acid (TFA) modulator, HCl and H_2O in the creation and stabilization of linker deficiencies with varying synthesis conditions – and afterwards during post-synthesis activation treatments with removal of linkers, dehydroxylation, *etc.*, whereby open accessible active Zr sites are created for catalysis. Most of the experimental findings, observed after synthesis and post-synthesis procedures, done by various experimental groups, have been confirmed by theory on the basis of pure energetic grounds. To the best of our knowledge, this is the first theoretical study where the formation of linker deficiencies under various synthesis conditions has been investigated in such a structural way.

An increase in the catalytic activity of the UiO-66 material and its variants can be due to a larger number of missing linkers in the structure or due to electronic effects induced by incorporating electron-withdrawing groups on the terephthalate linkers. Experimentally, it is not always trivial to discriminate between these two features, making theoretical calculations very challenging and complementary to the experiment. The two features can even be combined to form the best performing catalyst. In this context, the calculations reveal the UiO-66–NO_2 compound, prepared using HCl and TFA in the reaction mixture, as the most active catalyst. This fully confirms what has been observed experimentally. Other variants, which are expected to perform equally well, have also been suggested but should be confirmed by experiment.

Below, we summarize the most relevant features related to the synthesis of UiO-66 and its variants which are valid for both experiment and theory:

(i) the coordination of two TFA groups instead of a standard BDC linker is quite favoured and its prevalence increases with increasing TFA : BDC concentration in the reaction mixture;

(ii) the addition of HCl to the synthesis reaction mixture promotes the occurrence of a larger variety of linker deficiencies (2HCl, TFA/HCl) and thus a larger number of defects;

(iii) the addition of HCl at low synthesis temperatures (<150 °C) enables the incorporation of Cl^- anions into the cluster replacing hydroxyl groups;

(iv) thermal activation removes most of the coordinating MDL species, creating more open Zr sites;

(v) thermal activation also promotes dehydroxylation or water removal and is competitive with removal of a coordinating TFA;

(vi) functionalization of the linkers can significantly affect the Lewis acid strength of the metal and thus the reaction rate constant.

Further, we proposed a pathway for the first dehydroxylation of the inner $Zr_6O_4(OH)_4$ bricks under activation conditions. A decoordination of a terephthalate linker precedes the formation of a released hydroxyl group that then undergoes a protonation with another hydroxyl group to split off water.

We also tested the activity for the citronellal cyclization towards isopulegol over the different variants of UiO-66 catalysts. At low activation temperatures, TFA traces remain in the framework and hence might have an extra electronic effect on the catalytic activity. We indeed found some slight enhancement effects in the reaction rate constant. In addition, a remarkable correlation could be established between the activation enthalpies and the Hirshfeld-e charges of the active Zr site, implying that we can use these charges as a predictive tool to estimate the activity of UiO variants with other substituents of the functionalized linkers.

The success of these theoretical calculations has revealed new complementary insights into the synthesis process and

 This journal is © The Royal Society of Chemistry 2014

opens a lot of perspectives in guiding experimentalists in the design of optimal catalysts.

Acknowledgements

M.V. acknowledges funding from the Scientific Research Foundation Flanders (FWO) for a postdoctoral fellowship. J.H., V.V.S. and D.D.V thank the FWO for funding (project number 3G048612). V.V.S., D.D.V. and M.W. acknowledge BELSPO in the frame of IAP-PAI P7/05. V.V.S. acknowledges funding from the European Research Council under the European Community's Seventh Framework Programme [FP7(2007–2013) ERC grant agreement number 240483]. The computational resources and services used in this work were provided by VSC (Flemish Supercomputer Center), funded by the Hercules Foundation and the Flemish Government – Department EWI.

Notes and references

1 G. Férey, *Chem. Soc. Rev.*, 2008, **37**, 191–214.
2 J. L. C. Rowsell and O. M. Yaghi, *Microporous Mesoporous Mater.*, 2004, **73**, 3–14.
3 S. Kitagawa, R. Kitaura and S. Noro, *Angew. Chem., Int. Ed.*, 2004, **43**, 2334–2375.
4 O. M. Yaghi, M. O'Keeffe, N. W. Ockwig, H. K. Chae, M. Eddaoudi and J. Kim, *Nature*, 2003, **423**, 705–714.
5 D. Farrusseng, S. Aguado and C. Pinel, *Angew. Chem., Int. Ed.*, 2009, **48**, 7502–7513.
6 J. Lee, O. K. Farha, J. Roberts, K. A. Scheidt, S. T. Nguyen and J. T. Hupp, *Chem. Soc. Rev.*, 2009, **38**, 1450–1459.
7 L. Ma, C. Abney and W. Lin, *Chem. Soc. Rev.*, 2009, **38**, 1248–1256.
8 A. Dhakshinamoorthy, M. Alvaro and H. Garcia, *Catal. Sci. Technol.*, 2011, **1**, 856–867.
9 A. Dhakshinamoorthy and H. Garcia, *Chem. Soc. Rev.*, 2012, **41**, 5262–5284.
10 M. Yoon, R. Srirambalaji and K. Kim, *Chem. Rev.*, 2012, **112**, 1196–1231.
11 A. Corma, H. Garcia and F. X. L. I. Xamena, *Chem. Rev.*, 2010, **110**, 4606–4655.
12 J. H. Cavka, S. Jakobsen, U. Olsbye, N. Guillou, C. Lamberti, S. Bordiga and K. P. Lillerud, *J. Am. Chem. Soc.*, 2008, **130**, 13850–13851.
13 V. Guillerm, S. Gross, C. Serre, T. Devic, M. Bauer and G. Ferey, *Chem. Commun.*, 2010, **46**, 767–769.
14 M. Kandiah, M. H. Nilsen, S. Usseglio, S. Jakobsen, U. Olsbye, M. Tilset, C. Larabi, E. A. Quadrelli, F. Bonino and K. P. Lillerud, *Chem. Mater.*, 2010, **22**, 6632–6640.
15 F. Vermoortele, R. Ameloot, A. Vimont, C. Serre and D. De Vos, *Chem. Commun.*, 2011, **47**, 1521–1523.
16 L. Valenzano, B. Civalleri, S. Chavan, S. Bordiga, M. H. Nilsen, S. Jakobsen, K. P. Lillerud and C. Lamberti, *Chem. Mater.*, 2011, **23**, 1700–1718.
17 F. Vermoortele, M. Vandichel, B. Van de Voorde, R. Ameloot, M. Waroquier, V. Van Speybroeck and D. E. De Vos, *Angew. Chem., Int. Ed.*, 2012, **51**, 4887–4890.
18 K. Leus, M. Vandichel, Y. Y. Liu, I. Muylaert, J. Musschoot, S. Pyl, H. Vrielinck, F. Callens, G. B. Marin, C. Detavernier, P. V. Wiper, Y. Z. Khimyak, M. Waroquier, V. Van Speybroeck and P. Van der Voort, *J. Catal.*, 2012, **285**, 196–207.
19 M. Vandichel, S. Biswas, K. Leus, J. Paier, J. Sauer, T. Verstraelen, P. Van Der Voort, M. Waroquier and V. Van Speybroeck, *ChemPlusChem*, 2014, **79**, 1183–1197.
20 S. Biswas and P. Van der Voort, *Eur. J. Inorg. Chem.*, 2013, 2154–2160.
21 Y. T. Huang, W. P. Qin, Z. Li and Y. W. Li, *Dalton Trans.*, 2012, **41**, 9283–9285.
22 M. L. Foo, S. Horike, T. Fukushima, Y. Hijikata, Y. Kubota, M. Takata and S. Kitagawa, *Dalton Trans.*, 2012, **41**, 13791–13794.
23 S. Devautour-Vinot, G. Maurin, C. Serre, P. Horcajada, D. P. da Cunha, V. Guillerm, E. D. Costa, F. Taulelle and C. Martineau, *Chem. Mater.*, 2012, **24**, 2168–2177.
24 C. Zlotea, D. Phanon, M. Mazaj, D. Heurtaux, V. Guillerm, C. Serre, P. Horcajada, T. Devic, E. Magnier, F. Cuevas, G. Ferey, P. L. Llewellyn and M. Latroche, *Dalton Trans.*, 2011, **40**, 4879–4881.
25 Q. Y. Yang, A. D. Wiersum, P. L. Llewellyn, V. Guillerm, C. Serred and G. Maurin, *Chem. Commun.*, 2011, **47**, 9603–9605.
26 M. Kim, S. J. Garibay and S. M. Cohen, *Inorg. Chem.*, 2011, **50**, 729–731.
27 G. Wissmann, A. Schaate, S. Lilienthal, I. Bremer, A. M. Schneider and P. Behrens, *Microporous Mesoporous Mater.*, 2012, **152**, 64–70.
28 M. Kim and S. M. Cohen, *CrystEngComm*, 2012, **14**, 4096–4104.
29 G. E. Cmarik, M. Kim, S. M. Cohen and K. S. Walton, *Langmuir*, 2012, **28**, 15606–15613.
30 W. Morris, C. J. Doonan and O. M. Yaghi, *Inorg. Chem.*, 2011, **50**, 6853–6855.
31 M. Kandiah, S. Usseglio, S. Svelle, U. Olsbye, K. P. Lillerud and M. Tilset, *J. Mater. Chem.*, 2010, **20**, 9848–9851.
32 S. Chavan, J. G. Vitillo, M. J. Uddin, F. Bonino, C. Lamberti, E. Groppo, K. P. Lillerud and S. Bordiga, *Chem. Mater.*, 2010, **22**, 4602–4611.
33 M. Kim, J. F. Cahill, H. H. Fei, K. A. Prather and S. M. Cohen, *J. Am. Chem. Soc.*, 2012, **134**, 18082–18088.
34 C. H. Lau, R. Babarao and M. R. Hill, *Chem. Commun.*, 2013, **49**, 3634–3636.
35 Z. Guo, C. Xiao, R. V. Maligal-Ganesh, L. Zhou, T. W. Goh, X. Li, D. Tesfagaber, A. Thiel and W. Huang, *ACS Catal.*, 2014, **4**, 1340–1348.
36 L. J. Shen, W. M. Wu, R. W. Liang, R. Lin and L. Wu, *Nanoscale*, 2013, **5**, 9374–9382.
37 L. B. Vilhelmsen and D. S. Sholl, *J. Phys. Chem. Lett.*, 2012, **3**, 3702–3706.
38 R. Kardanpour, S. Tangestaninejad, V. Mirkhani, M. Moghadam, I. Mohammadpoor-Baltork, A. R. Khosropour and F. Zadehahmadi, *J. Organomet. Chem.*, 2014, **761**, 127–133.
39 J. Zhu, P. C. Wang and M. Lu, *Appl. Catal., A*, 2014, **477**, 125–131.

40 H. Wu, Y. S. Chua, V. Krungleviciute, M. Tyagi, P. Chen, T. Yildirim and W. Zhou, *J. Am. Chem. Soc.*, 2013, **135**, 10525–10532.
41 F. Vermoortele, B. Bueken, G. Le Bars, B. Van de Voorde, M. Vandichel, K. Houthoofd, A. Vimont, M. Daturi, M. Waroquier, V. Van Speybroeck, C. Kirschhock and D. E. De Vos, *J. Am. Chem. Soc.*, 2013, **135**, 11465–11468.
42 P. Xydias, I. Spanopoulos, E. Klontzas, G. E. Froudakis and P. N. Trikalitis, *Inorg. Chem.*, 2014, **53**, 679–681.
43 G. C. Shearer, S. Chavan, J. Ethiraj, J. G. Vitillo, S. Svelle, U. Olsbye, C. Lamberti, S. Bordiga and K. P. Lillerud, *Chem. Mater.*, 2014, **26**, 4068–4071.
44 A. Schaate, P. Roy, A. Godt, J. Lippke, F. Waltz, M. Wiebcke and P. Behrens, *Chem. – Eur. J.*, 2011, **17**, 6643–6651.
45 H. Furukawa, F. Gandara, Y. B. Zhang, J. C. Jiang, W. L. Queen, M. R. Hudson and O. M. Yaghi, *J. Am. Chem. Soc.*, 2014, **136**, 4369–4381.
46 W. B. Liang, H. Chevreau, F. Ragon, P. D. Southon, V. K. Peterson and D. M. D'Alessandro, *CrystEngComm*, 2014, **16**, 6530–6533.
47 M. J. Katz, Z. J. Brown, Y. J. Colon, P. W. Siu, K. A. Scheidt, R. Q. Snurr, J. T. Hupp and O. K. Farha, *Chem. Commun.*, 2013, **49**, 9449–9451.
48 F. Ragon, P. Horcajada, H. Chevreau, Y. K. Hwang, U. H. Lee, S. R. Miller, T. Devic, J. S. Chang and C. Serre, *Inorg. Chem.*, 2014, **53**, 2491–2500.
49 M. J. Cliffe, W. Wan, X. Zou, P. A. Chater, A. K. Kleppe, M. G. Tucker, H. Wilhelm, N. P. Funnell, F. X. Coudert and A. L. Goodwin, *Nat. Commun.*, 2014, **5**, 4176.
50 S. Jakobsen, D. Gianolio, D. S. Wragg, M. H. Nilsen, H. Emerich, S. Bordiga, C. Lamberti, U. Olsbye, M. Tilset and K. P. Lillerud, *Phys. Rev. B: Condens. Matter Mater. Phys.*, 2012, **86**, 125429.
51 O. Kozachuk, I. Luz, F. X. L. I. Xamena, H. Noei, M. Kauer, H. B. Albada, E. D. Bloch, B. Marler, Y. M. Wang, M. Muhler and R. A. Fischer, *Angew. Chem., Int. Ed.*, 2014, **53**, 7058–7062.
52 U. Ravon, M. Savonnet, S. Aguado, M. E. Domine, E. Janneau and D. Farrusseng, *Microporous Mesoporous Mater.*, 2010, **129**, 319–329.
53 G. C. Shearer, S. Forselv, S. Chavan, S. Bordiga, K. Mathisen, M. Bjorgen, S. Svelle and K. P. Lillerud, *Top. Catal.*, 2013, **56**, 770–782.
54 G. Mills, H. Jonsson and G. K. Schenter, *Surf. Sci.*, 1995, **324**, 305–337.
55 G. Henkelman, B. P. Uberuaga and H. Jónsson, *J. Chem. Phys.*, 2000, **113**, 9901–9904.
56 Y. Y. Liu, S. Couck, M. Vandichel, M. Grzywa, K. Leus, S. Biswas, D. Vollmer, J. Gascon, F. Kapteijn, J. F. M. Denayer, M. Waroquier, V. Van Speybroeck and P. Van der Voort, *Inorg. Chem.*, 2013, **52**, 113–120.
57 T. Verstraelen, P. W. Ayers, V. Van Speybroeck and M. Waroquier, *J. Chem. Theory Comput.*, 2013, **9**, 2221–2225.
58 H. Wu, T. Yildirim and W. Zhou, *J. Phys. Chem. Lett.*, 2013, **4**, 925–930.
59 M. Vandichel, F. Vermoortele, S. Cottenie, D. E. De Vos, M. Waroquier and V. Van Speybroeck, *J. Catal.*, 2013, **305**, 118–129.
60 C. Hansch, A. Leo and R. W. Taft, *Chem. Rev.*, 1991, **91**, 165–195.

 This journal is © The Royal Society of Chemistry 2014